HIFiRE-1 BOUNDARY LAYER TRANSITION MEASUREMENTS

Roger Kimmel*, David Adamczak*, Scott Stanfield, DSTO AVD Brisbane Team†**
***Air Force Research Laboratory, **Spectral Energies, LLC, †Defence Science and Technology Organisation, Air Vehicles Division**

Keywords: *hypersonics, boundary layer transition*

Abstract

The Hypersonic International Flight Research Experimentation (HIFiRE) program is a hypersonic flight test program executed by the United States Air Force Research Laboratory (AFRL) and the Australian Defence Science and Technology Organisation (DSTO). Flight one obtained hypersonic transition data showing four distinct transition phenomena: second-mode, roughness-induced, cross-flow and windward side transition. Cross-flow vortices may have been observed prior to the cross-flow transition. Wind tunnel tests and computations are suggested to better understand the flight data and to calibrate transition prediction tools to the flight environment.

1 Introduction

HIFiRE is a hypersonic flight test program executed by the United States AFRL and the Australian DSTO.[1,2] HIFiRE flight one occurred in March 2010. Its purpose is to develop and validate technologies critical to next generation hypersonic aerospace systems. Candidate technology areas include, but are not limited to, propulsion, propulsion-airframe integration, aerodynamics and aerothermodynamics, high temperature materials and structures, thermal management strategies, guidance, navigation, and control, sensors, and system components. The HIFiRE program consists of extensive ground tests and computation focused on specific hypersonic flight technologies. Each technology program is designed to culminate in a flight test. The first science flight of the HIFiRE series, HIFiRE-1, launched 22 March 2010 at the Woomera Prohibited Area in South Australia at 0045 UTC (1045 local time).

The primary objective of HIFiRE-1 was to measure aerothermal phenomena in hypersonic flight. The primary experiment consisted of boundary-layer transition measurements on a 7-deg half angle cone with a nose bluntness of 2.5 mm radius. The secondary aerothermal experiment was a shock-boundary-layer interaction created by a 33-deg-flare / cylinder configuration. HIFiRE-1 ground test and computation created an extensive knowledge base regarding transition on axisymmetric bodies. This research has been summarized in numerous prior publications.[3,4,5,6,7,8,9,10,11,12,13,14] Several papers describe the HIFiRE flight one mission. [15, 16, 17, 18] Ref. 16 presents an overview of preliminary results on smooth body and roughness-induced transition at low angle of attack, and smooth-body transition at high angle of attack. Ref. 16 further expands on the re-entry transition at high angle-of-attack. Since the ascent-phase transition is summarized thoroughly in Ref. 16, the current paper offers a high-level summary of these data, and a comparison to PSE calculations. The descent phase transition is a more complex process and has undergone additional study since Ref. 16 was published, so it is described in more detail.

The HIFiRE-1 flight data appear to display at least four distinct hypersonic transition phenomena. The ascent data appear to show low angle-of-attack, smooth-body second mode transition and transition due to isolated roughness. The entry transition data appear to demonstrate two more phenomena, cross-flow and windward-side forward transition. Subsequent analysis showed the windward-side reentry transition to be consistent with a second-mode-induced transition. [19] The HIFiRE-1 data offer an opportunity for synergistic interaction with wind tunnel test and

computations. Additional computation and wind tunnel tests are required to more fully understand the HIFiRE-1 data. The HIFiRE-1 data also offer an opportunity to calibrate hypersonic transition prediction and wind tunnel methods against the flight transition measurements.

2 Vehicle and Trajectory

The HIFiRE-1 vehicle has been described in several prior publications, most notably in Ref. 14. The overall payload dimensions and the different payload modules are shown in Fig. 1. The experiments were carried out on the forward sections of payload including a cone, a cylinder, and a flare which transitions to the diameter of the second stage motor (0.356 m). The cone half angle of seven degrees was chosen to match configurations used in preceding ground tests and analytical/numerical work. One side of the cone, the ϕ=180 deg. ray, incorporated a diamond-shaped trip element, 10 mm square and centered at x=0.5263 m.

The payload flew a ballistic trajectory similar to those employed for the HyShot [20] flights. The Terrier first stage burned for 6.3 seconds and then drag-separated from the second stage. The Orion/payload stack coasted until the second stage ignited at 15 seconds. Orion burnout occurred at 43 seconds. The payload remained attached to the second stage throughout the entire flight to provide stability as the payload reentered the atmosphere. Approximately the first and last 45 seconds of the trajectory were endoatmospheric. The

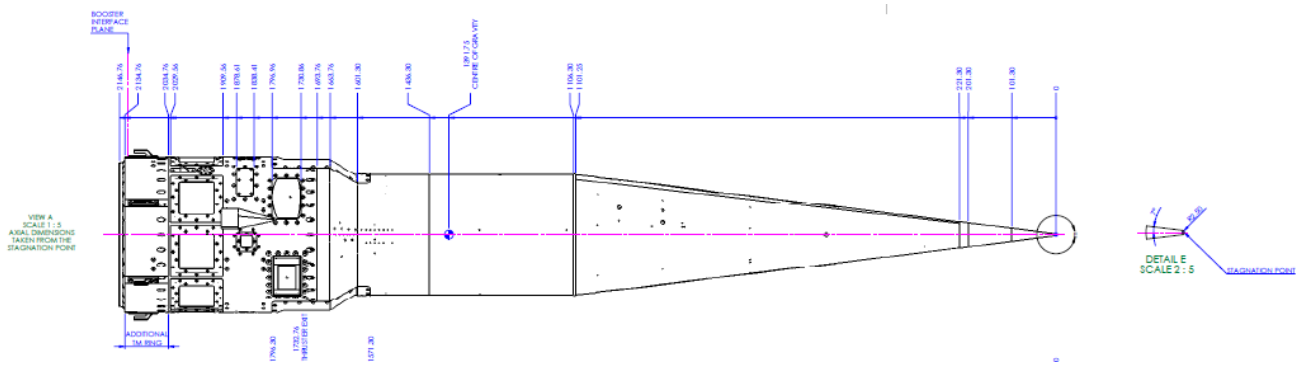

Fig. 1 HIFiRE-1 configuration

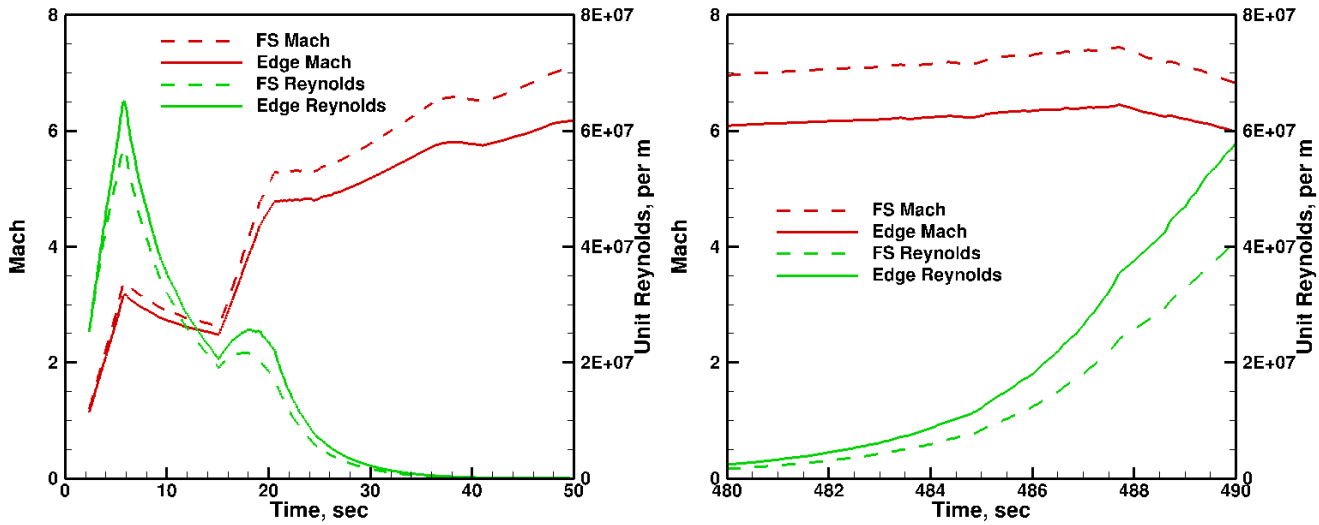

Fig. 2 Freestream and boundary layer edge Mach and Reynolds during ascent (left) and descent (right) portions of flight

remainder of the trajectory was exoatmospheric.

During exoatmospheric flight the vehicle was to have been reoriented with the reentry flight path angle. This was to have been accomplished using two nitrogen cold gas thrusters and a process employed for the reorientation of spinning satellites as presented by Wiesel.[21] Fig. 2 illustrates the edge and freestream Mach and Reynolds numbers during vehicle ascent and descent

The most notable mission complications were failures of the on-board GPS and the exoatmospheric pointing maneuver, and drift in the cone thermocouples. The loss of the GPS meant that the vehicle altitude and velocity had to be reconstructed from existing data such as accelerometers, radar tracks, etc. The failure of the exoatmospheric pointing maneuver caused the vehicle to enter the atmosphere with an angle of attack as high as 40-deg. Six-degree-of-freedom (6DOF) simulations and flight data indicate that the vehicle experienced oscillations in pitch, but that the oscillation amplitude and the overall AoA decreased at lower altitudes. However, the payload was still over 10-deg AoA as aerothermal data began to be collected during descent. Although descent was the intended design point for HIFiRE-1, at least a portion of the ascent yielded useful, low angle-of-attack data. Although the AoA complicated analysis of the descent data, this phase of the flight appears to have yielded useful high AoA transition data.

Angle of attack was estimated by taking local extrema in pressure for each transducer, and then interpolating AoA from tabulated values of cone pressure and Mach number. The estimated AoA was then obtained by averaging over the transducers. Fig. 3 illustrates these results. During ascent, AoA was less than 0.5 deg for t<21 seconds, and less than 1-deg for t<22 seconds. During descent, AoA varied from 5-13 deg for 482 < t < 485 seconds. The estimated uncertainty for AoA is 0.3-deg for ascent (t<22 sec) and 2.7 deg for descent (t>483 sec). This uncertainty is derived from the RMS variation in calculated AoA among the transducers. The oscillations in AoA shown in Fig. 3 are not measurement noise, but they are primarily due to damped pitch oscillations arising from the vehicle aerodynamics.

3.0 Ascent Transition

Ascent smooth-side transition may be divided into three phases. In the first phase, transition occurred near the nose tip, immediately after launch. This transition was probably caused by the backward-facing steps between the nose tip assembly and the aluminum body frustum. These steps were intentionally designed into the vehicle to accommodate differential thermal expansion among the nose-tip materials. During the second phase, transition moved rearward over

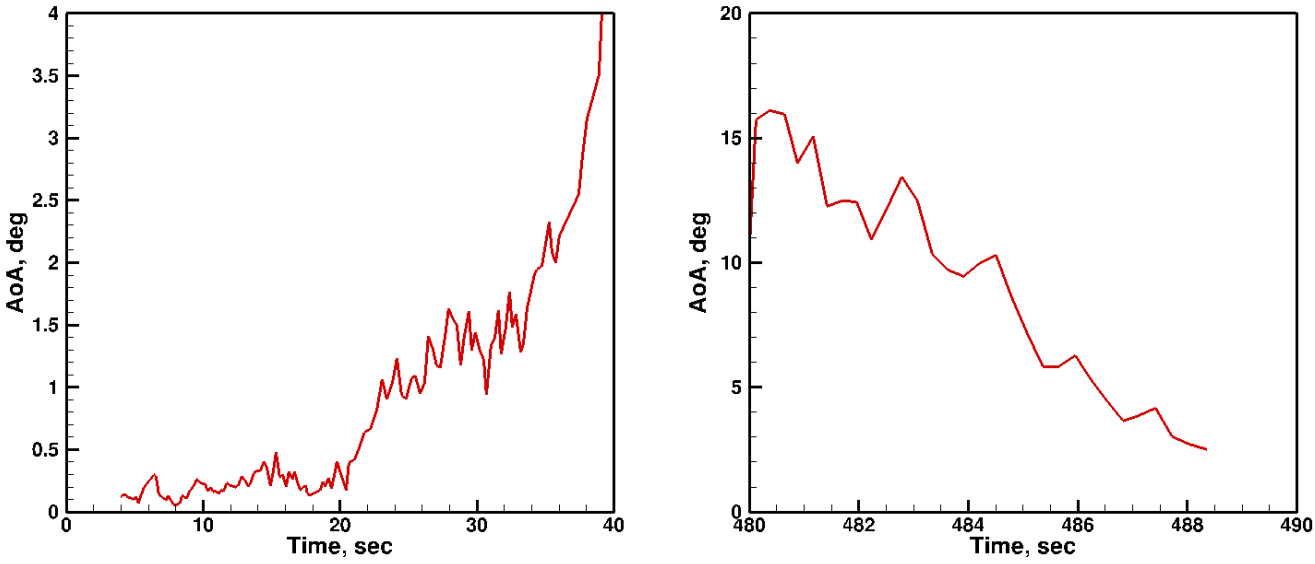

Fig. 3 HIFiRE-1 angle of attack during ascent (left) and descent (right).

the vehicle at a more gradual pace, although this progress was somewhat erratic. After the period of erratic transition movement, the transition front moved aft on the body at a steady rate, with good radial symmetry during the third phase of transition.[16]

At about t=11.5 seconds, the ϕ=180-deg ray (rough side) transitioned to laminar flow upstream of the trip element. Flow downstream of the trip was turbulent. Transducers downstream of the trip element recorded transitional or turbulent flow until about t=30 seconds. At approximately t=14 seconds, ϕ=0-deg (smooth-side) thermocouples upstream of x=0.6513 dropped from turbulent to laminar heat transfer values. The thermocouples on each ray that transitioned to laminar flow did so nearly simultaneously. This rapid transition front movement, commonly referred to as "flash-back," is typical of tripped transition.

Between about t=14 and t=19 seconds, the transition front moved aft on the body at a more gradual pace, but this process was somewhat intermittent. Transducers in the transitional zone showed large changes in heat transfer, oscillating between nearly turbulent and nearly laminar values before relaxing to consistently laminar levels. The cause of this behavior is unknown, but may be related to the nose-tip steps.

After t=19 seconds, the transition front moved aft until flow over the cone was fully laminar. The last thermocouple on the cone at x=1.0513 meters showed fully laminar heat transfer at t=22.5 seconds. Sample heat transfer distributions during this period are compared to PSE N-factor calculations [17] in Fig. 4. These comparisons indicate that second-mode N-factors at transition were about 14-15. Since determining transition from the heat transfer x-distributions is somewhat imprecise, correlating N-factors were determined by fitting a least-squares curve to transition times determined from individual transducer time-histories. This comparison indicated a second-mode correlating N-factor of 14. [17]…

4.0 Descent Transition

Interpretation of the descent transition is more complicated due to the high AoA during this period. The AoA created an azimuthally non-uniform transition front that progressed from the back of the vehicle forward over time.

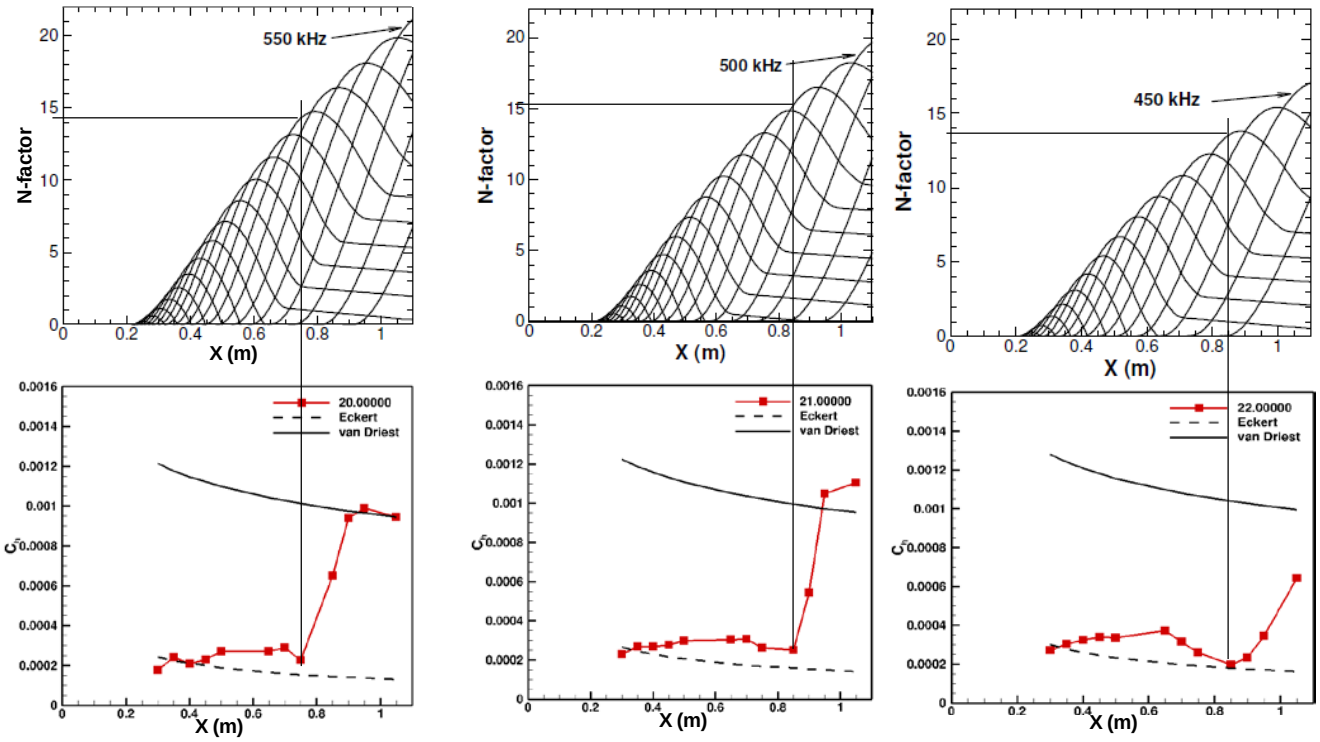

Fig. 4 N-factor calculations [17] and heat transfer distributions during ascent.

As the vehicle spun, individual transducers in the transitional region transited regions of laminar and turbulent flow. The Kulite pressure transducers and Vatell heat transfer gauges had response rates sufficient to resolve these passages between laminar and turbulent flow. The slower-response Medtherm coaxial thermocouples and Schmidt-Boelter gauges showed some modulation from the transition events, but data from these transducers are harder to characterize due to their damped response. The mean transition location derived from the thermocouples is described in Ref. 16. Therefore, the descent transition analysis will focus on the Kulites and Vatell gauges. Fig. 6 illustrates the relative location of these gauges.

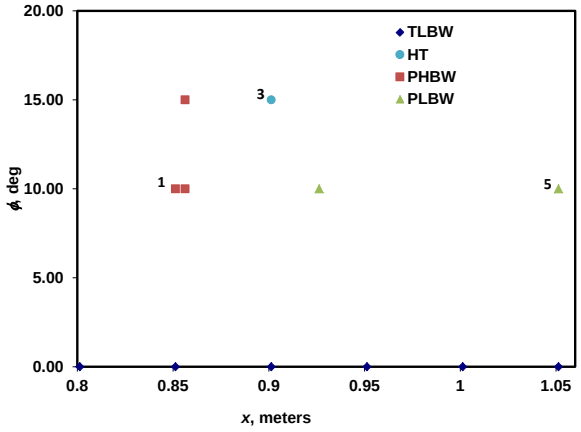

Fig. 6 High-bandwidth heat transfer and pressure instrumentation for entry analysis.

Several phenomena during the vehicle descent are of interest and are described in this section of the paper. First, the boundary layer on the lee side of the vehicle separated at higher angles of attack. Second, low-frequency periodic fluctuations in pressure and heat transfer occurred prior to transition. These fluctuations occurred near the shoulder of the vehicle at about Φ=90-deg, where Φ is the transducer instantaneous roll angle relative to the windward meridian. Third, two distinct transition zones appeared on the vehicle. One zone was related to the regions of periodic fluctuations near the shoulder of the cone. The other appeared on the windward side of the cone. The circumferential extent of these two regions increased with Reynolds number, until they merged to form fully turbulent flow around the circumference of the cone.

A critical factor in interpreting the re-entry data was determination of the roll angle of a transducer with respect to the windward meridian. The HIFiRE vehicle contained magnetometers and horizon sensors to measure roll relative to the earth. The instantaneous roll angle relative to the wind was determined using low-bandwidth pressure transducers on the cone and cylinder. Fig. 5 illustrates pressure measured on the cone. The cone pressures are generally sinusoidal in nature, with some distortion due to the boundary layer separation. The separation is manifested as a kind of clipping of the low-pressure (leeward) portion of the signal, with a local maximum on the leeward meridian and two minima on either side of this. Stetson [22] noted similar behaviour in wind tunnel experiments on cones at angle of attack. Comparison of surface oil-flow images to the pressures in Ref. 22 indicated that this type of pressure signature was present when the boundary layer separated, and that the separation occurred in-board of the minima. Separation did not necessarily occur in the presence of this double-minima feature, especially when the pressure gradients were small. Stetson did observe separation at values of α/θ_c as low as 0.7, so the HIFiRE cone flow was most likely separated prior to about 485-486 seconds.

A Hilbert transform [18] was applied to the pressure to determine the instantaneous phase of the pressure signal, and thus the roll location of

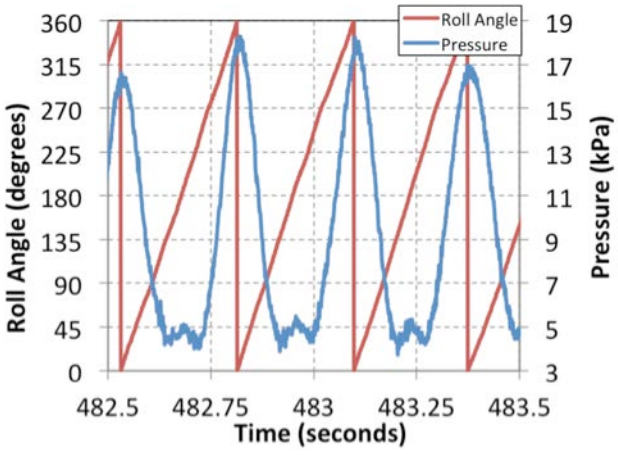

Fig. 5 Cone surface pressure and roll angle [18].

the transducer. Roll angle derived from the Hilbert transform is also illustrated in Fig. 5. The phase angle is nearly linear in time, indicating a nearly constant roll rate. The roll rate during descent decreased slowly from 4.2 Hz at t = 475 seconds to 3.3 Hz at t = 485 seconds. During one roll period, the maximum variation in Reynolds number was about 10%, and the maximum variation in angle of attack was about 0.3-degrees.

The transducer roll location process described above permits points from time-series data to be mapped into azimuthal locations around the vehicle circumference. Fig. 7 shows fluctuating pressures measured by high-bandwidth Kulite transducer PHBW1 over one cycle of rotation, from windward to leeward and back to windward again. The Φ=180-deg meridian is the lee side of the vehicle, and the Φ = 0 / 360 deg meridian is the wind side. The top axis of the graph shows the time-domain extent of the data, from 483.9-484.2 seconds. This portion of signal was chosen since it illustrates three phenomena observed in the high-bandwidth transducers during re-entry. These phenomena are (a) periodic pressure fluctuations near the model shoulders, (b) quiescent regions with low-amplitude fluctuations and (c) high-amplitude, non-periodic fluctuations near the vehicle centerline.

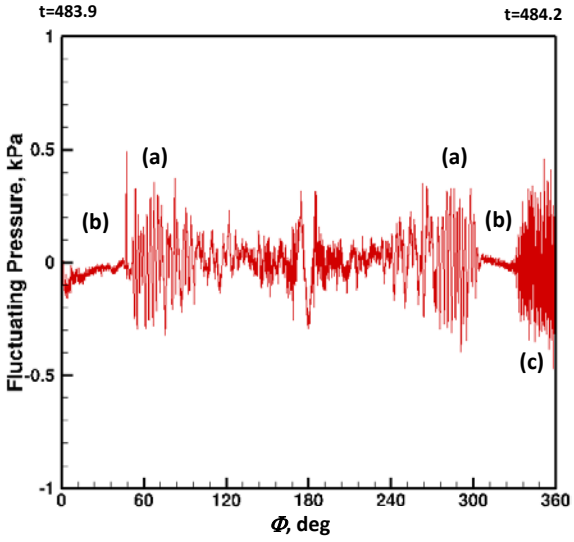

Fig. 7 High-bandwidth pressure time-series data converted to azimuthally-oriented data.

Inspection indicates region (a) as being laminar but unsteady, (b) as being laminar and (c) as turbulent.

This interpretation of laminar, transitional and turbulent regions of flow is supported by spectral analysis of the pressure transducer data and by high-bandwidth heat transfer measurements. Fig. 8 presents power spectra for the three regions identified in Fig. 7. Two unstable (a)-regions and two laminar (b)-regions are identifiable in Fig. 7, but Fig. 8 presents analysis only for portions of the rotation between 180 and 360-deg. Region (a) shows a pronounced spectral peak at about 300 Hz, and relatively low amplitude in the rest of the spectrum. Region (b) shows the lowest-amplitude signal across the spectrum. Region (c) shows a relatively flat spectrum that begins to drop off above about 5 kHz. These spectral signatures are consistent with an interpretation of these regions as unstable, laminar and turbulent respectively.

It should be noted that Fig. 7 represents the first appearance of windward side transition at this transducer location during descent. Prior to this time, the pressure signal at this location indicated laminar flow on the windward side of the vehicle on either side of the windward meridian. Presumably the Reynolds number increased sufficiently between 483.9 seconds to 484.2 seconds to support turbulent flow on the windward meridian. This transition occurred rather abruptly, with no preceding indication of unsteady fluctuations. Predicted second-mode

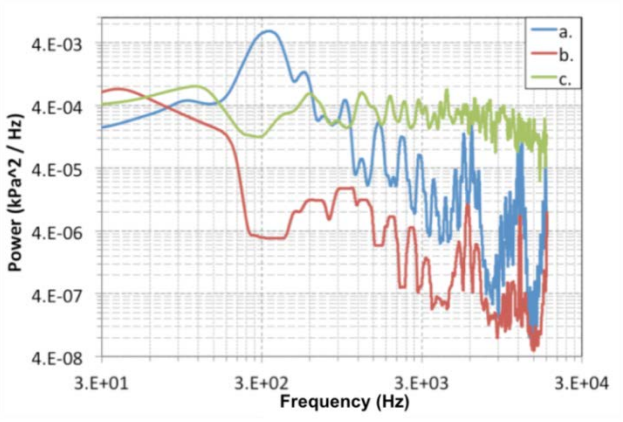

Fig. 8 Power spectra of pressure transducer data in Fig. 7 [18]

frequencies far exceeded the transducer bandwidth. [17]

Heat transfer measurements using the Vatell heat transfer gauge, HT3, also support the interpretation of the PHBW1 output. The HT3 gauge displayed a zero-shift during exoatmospheric flight. The HT3 output was shifted to zero at t=460 to compensate for this. The HT3 output is thus only qualitative, but transition trends may still be extracted from it. Fig. 9 shows the output for the HT3 for the roll period immediately preceding that shown in Fig. 7. This is the first point at which windward side transition is measured on the HT3 gauge. Windward side transition occurs at this gauge before it is observed on PHBW1, since PHBW1 was upstream of HT3, and the transition front is moving from the rear of the cone forwards. The HT3 gauge output is qualitatively similar to the PHBW1 output, with regions of apparently undisturbed flow flanking regions of transitional flow centered at about 90 and 270-deg.

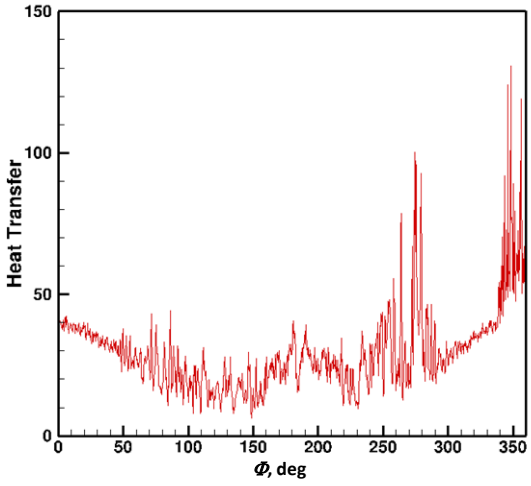

Fig. 9 HT3 heat transfer gauge output for period beginning at t=483.6532 sec showing first windward side transition at this location

The root-mean square (RMS) pressure fluctuations may be plotted in a contour plot with azimuthal location and Reynolds number as axes to visualize the 3D transition front. RMS pressures were computed by applying a 0.007-second moving window to the PHBW1 pressure transducer output. These RMS pressures were normalized by the local mean pressure, measured with an adjacent low-bandwidth pressure transducer. These results are presented in contour format in Fig. 10. It should be noted that the vehicle is undergoing changes in AoA during this period. AoA decreased from about 15-deg at the lowest Reynolds numbers to about 5-deg at the highest Reynolds. The most prominent features in this contour plot are a region of elevated fluctuations on the lee side, lobes of relatively high-amplitude fluctuations around the shoulders of the vehicle, and a windward-side transition.

The squares in Fig. 10 indicate the locations of pressure minima on the lee side of the cone. The separated region is contained within this region. Pressure fluctuations occurred here even at the lowest Reynolds number where reliable data can be extracted. It is unclear if these fluctuations are due to unsteady separation or transition, but the normalized RMS in this region peaked at a Reynolds number of about $4x10^6$.

The diamonds in Fig. 10 encompass two regions of periodic pressure fluctuations. Analysis showed the derived wavenumber of these fluctuations to be consistent with stationary cross-flow vortices. [17] These lobes are centered at about Φ =90 and 270 deg. These periodic fluctuations were first discernible at a Reynolds number just above $2x10^6$. The relative fluctuation level increases with Reynolds number until reaching a maximum of about 2.6% at Re=$3.2\text{-}3.6x10^6$. Since AoA was decreasing during this period, it is unclear whether this local maximum in RMS was due to the transition process or variations in AoA. The region grew in azimuthal extent until a Reynolds number of about $4x10^6$. Until this time the inboard extent of the region was sharply circumscribed by the pressure minima. As Reynolds number increased beyond $4x10^6$, the windward limit of the region remained at about 45 deg. Transition propagated from the lee side of the vehicle. By Re=$5.6x10^6$ the region was largely turbulent.

The triangles in Fig. 10 indicate windward-side transition. Windward-side transition commenced at a Reynolds number of about $5x10^6$. This turbulent region spread azimuthally until it merged with the periodic fluctuations at about Re= $5.6x10^6$. At this point the flow appeared to be fully turbulent around the

circumference of the vehicle at this location. Normalized RMS pressure levels peaked at about 1% near the beginning of the windward transition, and decrease after this. Ascent data showed turbulent fluctuations to be typically 0.3%, peaking up to 1.25% during transition. Immediately after ascent transition, fluctuation levels dropped to 0.1%. This fluctuation level also contained a contribution from electronic noise, estimated to be roughly 0.02%, based on

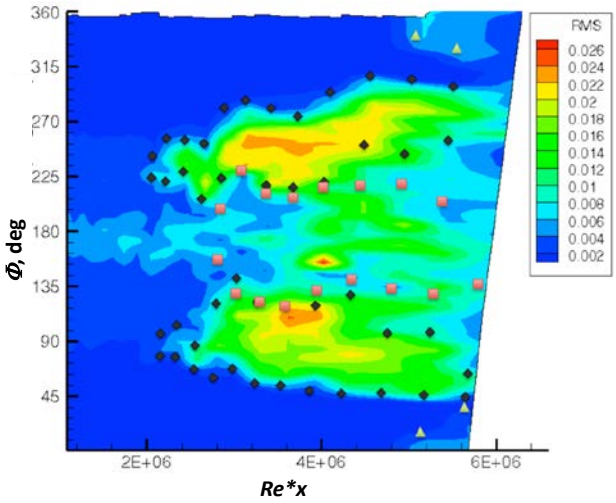

Fig. 10 Contour plot of RMS pressure fluctuations for transducer PHBW1. Squares: leeward side mean pressure minima, diamonds: limits of periodic pressure fluctuations, triangles – limit of windward side transition. [18]

RMS levels measured during exoatmospheric flight. It should be noted that the pressure transducer pass band is insufficient to capture second mode or the full turbulent spectrum, so actual RMS pressure levels were in some cases probably higher than measured.

The transition front on the vehicle measured by the PHBW1 and HT3 gauges and mapped into Reynolds number and circumferential location is illustrated in Fig. 11. The black line indicates the transition front. Blue diamond and orange circle symbols respectively illustrate the regions of pressure and heat transfer fluctuations. Periodic pressure fluctuations existed in the blue-shaded region. Red squares indicate the local pressure minima. The region between them, shaded red, was largely separated. The upstream and downstream extent of this region is not well defined. The boundary layer state (laminar or turbulent) within this region is difficult to define due to the low heat transfer levels and unsteady flow within it. The green triangles indicate the windward side transition as measured by the pressure gauges. They are largely coincident with the transition front measured from the heat transfer gauge. Fig. 11 gives the overall impression of periodic disturbances around the shoulder of the model preceding a transition front that spreads from the lee side of the model. This transition process is consistent with wind tunnel observations of cross flow transition. Windward transition appears rather abruptly and propagates leeward to merge with the cross-flow transition.

5.0 Conclusion and Recommendations

The HIFiRE-1 test garnered data on four distinct transition phenomena in hypersonic flight. The ascent provided low-angle-of-attack, smooth-body, second-mode transition, and tripped transition. Cross-flow and windward side transition occurred during descent. These data present an opportunity for interaction with ground test and computation. Wind tunnel tests and computation can help us understand the transition mechanisms on HIFiRE-1. At the same time, the flight can provide calibration for empirical and computational predictions, and help to validate their underlying assumptions.

Ascent transition, which occurred at low

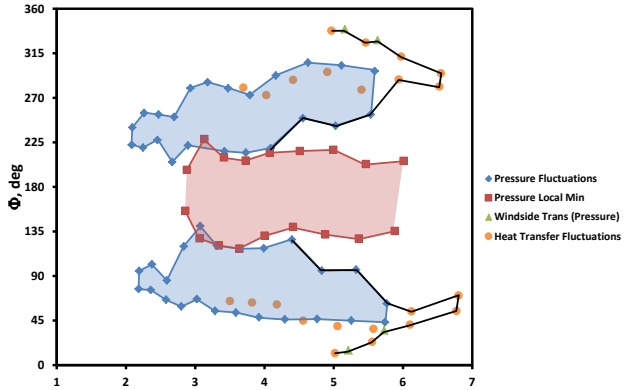

Fig. 11 Regions of elevated heat transfer and pressure fluctuations and transition front. Black line indicates transition front.

angle of attack, was correlated with a second-mode N-factor of 14 [17]. This value probably represents an upper bound on the correlating N-factor for second-mode transition in flight on a smooth, non-ablating, non-reacting surface. Tripped transition data acquired during ascent has only received a limited amount of analysis. These data would benefit from more detailed analysis to derive correlating roughness parameters, such as roughness Reynolds numbers that could be used to extrapolate wind tunnel data and aid in vehicle design.

The cross-flow transition during descent was preceded by periodic pressure and heat transfer fluctuations that appear to be a signature of cross-flow instability. If wind tunnel tests and computations support this supposition, this finding would permit linear-stability-based transition prediction methods to be applied to flight conditions with greater confidence. Descent transition data may yield insight into crossflow transition criteria for hypersonic flight. The windward side transition observed during descent has been observed to a limited degree in wind tunnel tests. Again, computations and experiment may shed more light on the mechanism causing this transition. In turn, observation of this mechanism in the flight environment would permit transition prediction with greater confidence.

6.0 Acknowledgments

The authors thank John Schmisseur of the Air Force Office of Scientific Research and Douglas Dolvin of the Air Force Research Laboratory for their support of this work. This work was supported by the United States Air Force Research Laboratory and the Australian Defence Science and Technology Organisation and was carried out under Project Agreement AF-06-0046. Many thanks are extended to Royal Australian Navy Ranges and Assessing Unit, Aerospace Operational Support Group of the Royal Australian Air Force and White Sands Missile Range/DTI/Kratos. Mary Bedrick of Detachment 3 Air Force Weather Agency provided the best-estimated atmosphere. Mark Smith of NASA Dryden Flight Research Center developed a best-estimated trajectory, and Thomas Squire of NASA Ames Research Center performed additional thermal analysis.

Copyright Statement

References

1 Dolvin, D. “Hypersonic International Flight Research and Experimentation (HIFiRE) Fundamental Science and Technology Development Strategy,” AIAA Paper 2008-2581, April 2008.

2 Dolvin, D. J., “Hypersonic International Flight Research and Experimentation Technology Development and Flight Certification Strategy,” AIAA paper 2009-7228, October 2009.

3 Kimmel, R. L., Adamczak, D., Gaitonde, D., Rougeux, A., Hayes, J. R., “HIFiRE-1 Transition Experiment Design,” AIAA paper 2007-0534, January 2007.

4 Wadhams, T. P., MacLean, M. G., Holden, M.S., and Mundy, E., “Pre-Flight Ground Testing of the Full-Scale FRESH FX-1 at Fully Duplicated Flight Conditions,” AIAA paper 2007-4488, June 2007.

5 Johnson, H. B., Alba, C. R., Candler, G. V., MacLean, M., Wadhams, T, and Holden, M. “Boundary Layer Stability Analysis of the Hypersonic International Flight Research Transition Experiments,” AIAA Journal of Spacecraft and Rockets, vol. 45, no. 2, March-April 2008.

6 Holden, M. S., Wadhams, T. P., MacLean, M., “Experimental Studies in the LENS Supersonic and Hypersonic Tunnels for Hypervelocity Vehicle Performance and Code Validation,” AIAA paper 2008-2505, April 2008.

7 Kimmel, R. L., “Aerothermal Design for the HIFiRE-1 Flight Vehicle,” AIAA paper 2008-4034, June 2008.

8 Casper, K. M., Wheaton, B. M., Johnson, H. B., and Schneider, S. P., “Effect of Freestream Noise on Roughness-Induced Transition at Mach 6,” AIAA paper 2008-4291 June 2008.

9 Kimmel, R. L., “Roughness Considerations for the HIFiRE-1 Vehicle,” AIAA Paper 2008-4293, June 2008.

10 Alba, C. R., Johnson, H. B., Bartkowicz, M. D., Candler, G. V., and Berger, K. T. "Boundary-Layer Stability Calculations for the HIFiRE-1 Transition Experiment," AIAA Journal of Spacecraft and Rockets, vol. 45, no. 6, November-December 2008, pp. 1125-1133.

11 Wadhams, T. P., Mundy, E., MacLean, M. G., and Holden, M. S., "Ground Test Studies of the HIFiRE-1 Transition Experiment Part1: Experimental Results," AIAA Journal of Spacecraft and Rockets, vol. 45, no. 6, November-December 2008, pp. 1134-1148.

12 MacLean, M., Wadhams, T., Holden, M., and Johnson, H., "Ground Test Studies of the HIFiRE-1 Transition Experiment Part 2: Computational Analysis," AIAA Journal of Spacecraft and Rockets, vol. 45, no. 6, November-December 2008, pp. 1149-1164.

13 Berger, K. T., Greene, F. A., Kimmel, R. L., Alba, C., and Johnson, H., "Erratum on Aerothermodynamic Testing and Boundary-Layer Trip Sizing of the HIFiRE Flight 1 Vehicle," AIAA Journal of Spacecraft and Rockets, vol. 46, no., 2, March-April, 2009, pp. 473-480.

14 Adamczak, D., Alesi, H., Frost, M., "HIFiRE-1: Payload Design, Manufacture, Ground Test, and Lessons Learned," AIAA paper 2009-7294, October 2009.

15 Adamczak, D., Kimmel, R. L., Paull, A., Alesi, H., "HIFiRE-1 Flight Trajectory Estimation and Initial Experimental Results," AIAA paper 2011-2358, May 2011

16 Kimmel, R. L., Adamczak, D., and Brisbane DSTO-AVD Team, "HIFiRE-1 Preliminary Aerothermodynamic Experiments," AIAA paper 2011-3414, June 2011.

17 Li, F., Choudhari, M., Chang, C., Kimmel, R., Adamczak, D., "Transition Analysis for the HIFiRE-1 Flight Experiment," AIAA paper 2011-3414, June 2011.

18 Stanfield, S. A., Kimmel, R. L., and Adamczak, D., "HIFiRE-1 Data Analysis: Boundary Layer Transition Experiment During Reentry," AIAA paper 2012-1087, January 2012

19 Li, F., Choudhari, M., Chang, C.-L., White, J., Kimmel, R., Adamczak, D., Borg, M., and Stanfield, S., "Stability analysis for HIFiRE Experiments, AIAA Paper 2012-2961, June 2012.

20 Smart, M. K., Hass, N. E., and Paull, A., "Flight Data Analysis of the HyShot 2 Scramjet Flight Experiment," AIAA Journal, vol. 44, no. 10, October 2006, pp. 2366-2375.

21 Wiesel W. E., Spaceflight Dynamics, 2nd Ed., McGraw-Hill Series in Aeronautical and Aerospace Engineering, McGraw-Hill, pp. 138-140, 1997.

22 Stetson, K. F., "Boundary-Layer Separation on Slender Cones at Angles of Attack," *AIAA Journal*, vol. 10, pp. 642-648, 1972.